COMPARATIVE ANALYSIS OF TIP VORTEX FLOW USING RANS AND LES

MARINE 2017

ABOLFAZL ASNAGHI, RICKARD E. BENSOW* AND URBAN SVENNBERG†

*Department of Shipping and Marine Technology
Chalmers University of Technology, Gothenburg, Sweden
e-mail: {abolfazl.asnaghi, rickard.bensow}@chalmers.se

†Rolls Royce AB, Kristinehamn, Sweden
e-mail: urban.svennberg@rolls-royc.com

Key words: Tip Vortex, Numerical Simulation, RANS, LES, Cavitation Inception

Abstract. The current study focuses on the numerical analysis of tip vortex flows, with the emphasis on the investigation of turbulence modelling effects on tip vortex prediction. The analysis includes comparison of RANS and LES methods at two different mesh resolutions. Implicit LES, ILES, modelling is employed here to mimic the turbulent viscosity. In RANS, the two equation k-ω SST model is adopted. In order to also address possible benefits of using streamline curvature variations in RANS, two curvature correction methods proposed for k-ω SST are tested, and compared. ILES results show very good agreement with the experimental observations. The predicted vortex in ILES is also stronger than RANS predictions. ILES has predicted accelerated vortex core axial velocity very well, while tested RANS models under predict the axial velocity. Adoption of curvature correction has not improved the tip vortex prediction, even though it has reduced the turbulent viscosity at the vortex core.

1 INTRODUCTION

As the flow passes over a lifting wing with finite span, close to the wing tip the pressure differential drives the fluid from the high pressure side on the lower surface to the low pressure side on the upper surface. This creates a highly rotational vortex flow pattern at the tip region. As this vortex is transported downstream more flow from the wake of the wing is fed into the vortex. This roll-up process will strengthen the vortex until its circulation is nominally equal to that of the wing. The roll-up process typically extends to a few wing spans downstream of the trailing edge, which is denoted the near field region. After this region and when the roll-up is finished, the vortex will start to decay due to the flow viscosity [1,2].

As the pressure at the vortex core is lower than the surrounding area, in the cavitating case, cavitation incepts at the vortex core. Understanding the physics of these flows, and its modelling, is therefore important in finding the tip vortex inception speed to prevent or control the occurrence of cavitation on propellers [3,4].

Experimental tests on propellers can provide very useful information about the vortex properties and the tip vortex cavitation inception. However, despite the huge cost which has to be spent for each test, as the tip vortex involves very small scale flow dynamics it is very

difficult to measure relevant flow features, e.g. velocity distribution, even by advanced measurements tools. Another drawback is the disability to measure the pressure at the vortex core where cavitation inception occurs. Numerical tools and CFD can be used to give further insights on the tip vortex properties that experimental tests may not be able to provide [5-7].

The current study focuses on the evaluation of different turbulence modelling approaches in prediction of tip vortex flows around an elliptical foil. The aim is to compare the k-ω SST RANS model and Implicit LES, which have been used widely in marine applications [8-11]. In the authors' previous study, mesh resolution requirements for tip vortex analysis in laminar and ILES methods have been conducted [2]. Here, the turbulence models are tested on the optimum spatial resolution. One coarser resolution is also considered to briefly address the impacts of turbulence modelling on different spatial resolutions.

Another objective of the paper is to compare two different curvature correction methods, and how they change the flow prediction in different spatial resolutions. It has been reported that linear eddy viscosity assumption is insensitive to the streamline curvature [12-14]. This leads to over-prediction of the turbulent viscosity in high swirling regions, e.g. the vortex core. As a result, the numerically predicted vortex decays much too fast. Curvature corrections are proposed, essentially for linear eddy viscosity based models such as k-ω SST, to cure over-prediction of the turbulent viscosity.

The simulations and analysis are conducted on the tip vortex flow on an elliptical foil, namely Arndt elliptical foil. The vortex structures around this type of foil resembles the propeller tip vortex behaviour while making it possible to be tested in more details both experimentally and numerically. The tip vortex at the selected operating conditions is relatively stationary which reduces the computational requirements [15, 16].

The investigations include the comparisons of vortex trajectory, vortex axial velocity at the vortex core, velocity distributions at different in-plane sections downstream of the foil, and the pressure distribution. Turbulent viscosity for different RANS models are also presented to evaluate the effects of curvature correction. Results indicate that ILES is capable of prediction of tip vortex characteristics very accurately in the near field region; accelerated vortex core axial velocity and in-plane velocity distribution matches quite well with experimental PIV images. The SST models, however, fail in correctly predicting the vortex properties. Even though the vortex properties of the RANS simulations, close to the tip, are similar to ILES, the predicted vortex fades very rapidly in RANS.

2 ELLIPTICAL FOIL

The current study focuses on the numerical investigation of the wetted flow of the Arndt elliptical foil. The geometry is an elliptical planform having the NACA $66_2 - 145$ as cross section having mean line equal to a = 0.8 [1,15-18]. In the current study, the experimental study conducted in the test tunnel of the Laboratory for Ship Hydrodynamics at Delft University is selected for comparison with the numerical results [15, 16]. In the experimental tests, Stereoscopic PIV measurements were employed to provide the velocity distributions at different sections downstream of the foil. Correlation averaging was utilized in the post processing of PIV images in order to minimize the interrogation area size. The foil was tested at different flow conditions; here, the wetted flow conditions with fixed inlet velocity (6.8 m/s) is employed while the foil has angle of attack equal to 9 degrees.

3 GOVERNING EQUATIONS

3.1 RANS Model

The conservation of momentum in RANS framework is,

$$\frac{\partial(\rho\overline{u_i})}{\partial t}+\frac{\partial(\rho\overline{u_i u_j})}{\partial x_j}=-\frac{\partial\overline{p}}{\partial x_i}+\frac{\partial}{\partial x_j}\left[(\mu+\mu_t)\frac{\overline{u_i}}{\partial x_j}\right]. \tag{1}$$

In the current study, k-ω SST model is used to model the turbulent viscosity. In k-ω SST, two transport equations for turbulent kinematic energy and dissipation terms are solved [12],

$$\frac{\partial(\rho k)}{\partial t}+\frac{\partial(\rho\overline{u_j}k)}{\partial x_j}=P-\beta^*\rho\omega k+\frac{\partial}{\partial x_j}\left[(\mu+\sigma_k\mu_t)\frac{\partial k}{\partial x_j}\right], \tag{2}$$

$$\frac{\partial(\rho\omega)}{\partial t}+\frac{\partial(\rho\overline{u_j}\omega)}{\partial x_j}=\frac{\gamma}{\upsilon_t}P-\beta\rho\omega^2+\frac{\partial}{\partial x_j}\left[(\mu+\sigma_\omega\mu_t)\frac{\partial\omega}{\partial x_j}\right]+2(1-F_1)\frac{\rho\sigma_{\omega2}}{\omega}\frac{\partial k}{\partial x_j}\frac{\partial\omega}{\partial x_j}, \tag{3}$$

$$P=\tau_{ij}\frac{\partial u_i}{\partial x_j}, \tag{4}$$

$$\tau_{ij}=\mu_t\left(2S_{ij}-\frac{2}{3}\frac{\partial u_k}{\partial x_k}\delta_{ij}\right)-\frac{2}{3}\rho k\delta_{ij}, \tag{5}$$

$$\mu_t=\frac{\rho a_1}{max(a_1\omega,\Omega F_2)}, \tag{6}$$

$$F_1=\tanh(arg_1^4),\ arg_1=min\left[max\left(2\frac{\sqrt{k}}{\beta^*\omega d},\frac{500\nu}{d^2\omega}\right),\frac{4\rho\sigma_{\omega2}k}{CD_{k\omega}d^2}\right] \tag{7}$$

$$F_2=\tanh(arg_2^2),arg_2=max\left(2\frac{\sqrt{k}}{\beta^*\omega d},\frac{500\nu}{d^2\omega}\right). \tag{8}$$

The constants are:

$$\gamma_1=\frac{\beta_1}{\beta^*}-\frac{\sigma_{\omega1}\kappa^2}{\sqrt{\beta^*}},\ \gamma_2=\frac{\beta_2}{\beta^*}-\frac{\sigma_{\omega2}\kappa^2}{\sqrt{\beta^*}},\ \sigma_{k1}=0.85,\ \sigma_{k2}=1.0,\ \sigma_{\omega1}=0.5,\ \sigma_{\omega2}=0.856,\ \beta_1=0.075,$$
$$\beta_2=0.0828,\ \beta^*=0.09,\ a_1=0.31,\ \kappa=0.41. \tag{9}$$

3.2 Curvature Correction

According to the Boussinesq eddy viscosity assumption, a linear relation between turbulent viscosity and the velocity strain rate is considered. This assumption is insensitive to the flow streamline curvature, thus, for highly swirling flows, this can lead to over prediction of turbulent viscosity in the swirling region. Various curvature corrections have been proposed to correct RANS models to also include the curvature variations [12-14].

3.2.1 Menter SST Two-Equation Model with Rotation/Curvature Correction (SST-RC) [12]

This curvature correction form of the SST model is the same as the standard version of SST, except that the production term P in both equations (i.e. transport of k and ω) gets multiplied by a function f_{r1},

$$f_{r1}=max[min\{f_{rotation},1.25\},0], \tag{10}$$

where

$$f_{rotation} = (1 + C_{r1})\frac{2r^*}{1+r^*}[1 - C_{r3}tan^{-1}(C_{r2}\hat{r})]\text{-}C_{r1}. \tag{11}$$

All the variables and their derivatives are defined with respect to the reference frame of the calculation, which may be rotating with rotation rate Ω^{rot}. Remaining functions are defined as,

$$r^* = \frac{S}{W}, \tag{12}$$

$$\hat{r} = \frac{2W_{ih}S_{jh}}{WD^3}\left(\frac{DS_{ij}}{Dt} + \left(\varepsilon_{imn}S_{jn} + \varepsilon_{jmn}S_{in}\right)\Omega_m^{rot}\right), \tag{13}$$

$$S_{ij} = \frac{1}{2}\left(\frac{\partial u_i}{\partial x_j} + \frac{\partial u_j}{\partial x_i}\right), \tag{14}$$

$$W_{ij} = \frac{1}{2}\left[\left(\frac{\partial u_i}{\partial x_j}\text{-}\frac{\partial u_j}{\partial x_i}\right) + 2\varepsilon_{mji}\Omega_m^{rot}\right], \tag{15}$$

$$S^2 = 2S_{ij}S_{ij}, \tag{16}$$

$$W^2 = 2W_{ij}W_{ij}, \tag{17}$$

$$D^2 = max(S^2, 0.09W^2), \tag{18}$$

$$C_{r1} = 1.0,\ \ C_{r2} = 2.0,\ \ C_{r3} = 1.0. \tag{19}$$

The term DS_{ij}/Dt represents the components of the material derivative of the strain rate tensor. The rotation rate, Ω^{rot}, is nonzero only if the reference frame itself is rotating.

3.2.2 Hellsten's Simplified Rotation/Curvature Correction (SST-RC-Hellsten) [13, 14]

In this simplified rotation/curvature form of the SST model, the destruction term in the ω equation, $\beta\rho\omega^2$, gets multiplied by the function F_4, and becomes, $F_4\beta\rho\omega^2$. The definition of F_4 is,

$$F_4 = \frac{1}{1+C_{RC}R_i}, \tag{20}$$

where

$$R_i = \frac{W}{S}\left(\frac{W}{S} - 1\right), \tag{21}$$

and C_{RC} is a constant equal to 1.4.

3.3 LES Model: Implicit LES

The filtered Navier-Stokes equation in LES framework is as follows,

$$\frac{\partial(\rho\overline{u_i})}{\partial t} + \frac{\partial(\rho\overline{u_i}\overline{u_j})}{\partial x_j} = -\frac{\partial\bar{p}}{\partial x_i} + \frac{\partial}{\partial x_j}\left(\overline{S_{ij}}\text{-}B_{ij}\right). \tag{22}$$

In this equation, $B_{ij} = \rho_m\left(\overline{u_i u_j}\text{-}\overline{u_i}\,\overline{u_j}\right)$ is the subgrid stress tensor and $S_{ij} = \mu\left(\partial u_i/\partial x_j + \partial u_j/\partial x_i\right)$ is the shear stress. In ILES model used in this study, no explicit function is applied for B; instead the numerical dissipation is considered enough to mimic the action of B [8-10].

4 COMPUTATIONAL DOMAIN

The computational domain employed here follows the dimensions of the cavitation tunnel at TU Delft. A fixed inlet velocity boundary and fixed outlet pressure boundary is used along with the slip condition on the other boundaries, Figure 1. The inlet velocity is set equal to 6.8 m/s which corresponds to the Reynolds number of 8.5e05. The outlet pressure is set fixed equivalent to cavitation number 4.2. For RANS computations, the inlet turbulence intensity is considered to be equal to 5%.

The inlet and outlet are located five chord length upstream, and ten chord length downstream of the foil. The foil is placed at the center of the channel width, where distance to each side is equal to 150 mm. The root chord length of the foil is equal to 125.6 mm. The center of the coordinate system is located at the center of the chord at the root, and as a result, all of the numerical results in this study are reported accordingly. The trailing edge has been cut off with a thickness of 0.3 mm, and the total area of the foil from the 3D CAD model is 0.01465 m^2 which is used as the reference area to compute non-dimensional parameters, e.g. lift coefficient. This corresponds to the situation at the experiments.

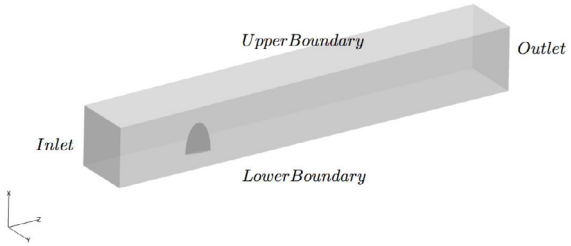

Figure 1: Boundary positions, Arndt foil

The tip vortex flows involve very small scales of the flow, both in time and space. Capturing these small scales of flow physics requires very fine computational resolution. The current study focuses on a condition that results in a relatively stationary tip vortex. This reduces the computational time required for the tip vortex to develop and evolve. However, as the vortex diameter is 1 mm, still very fine spatial resolution is required to predict the tip vortex and the flow surrounding it. In previous studies conducted by the authors, a mesh independency study was performed to find appropriate mesh resolution to predict the tip vortex in the near field region, i.e. 1.5 chord lengths downstream of the tip. This distance is deemed appropriate as the main concern of the research is to investigate the tip vortex cavitation inception and its relation with the tip vortex characteristics.

In Figures 2 and 3, general distribution of the cells in the streamwise and in-plane directions are presented. The computational cells are fully hexahedral, generated by employing StarCCM+ of CD-Adapco. Different refinement regions are defined to refine the resolution up to the tip vortex region.

In Table 1, specifications of two mesh resolutions are presented. P1S1 is the coarsest resolution tested in previous studies, and P2S2Wake is the resolution found to be adequate to predict the tip vortex in the near field region [2]. In one of the previous studies, the flow is treated as a laminar flow, and in the other one, ILES was employed. As the tip vortex core has a diameter equal to 1 mm, the sizes in this table are presented accordingly.

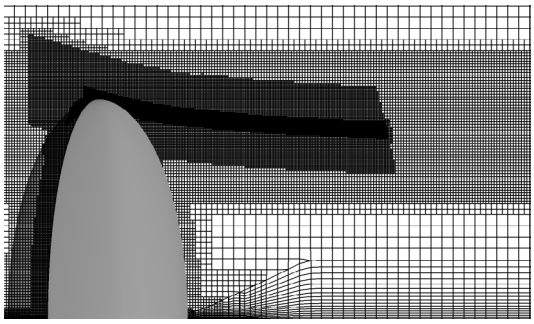

Figure 2: Streamwise mesh distribution, P1S1

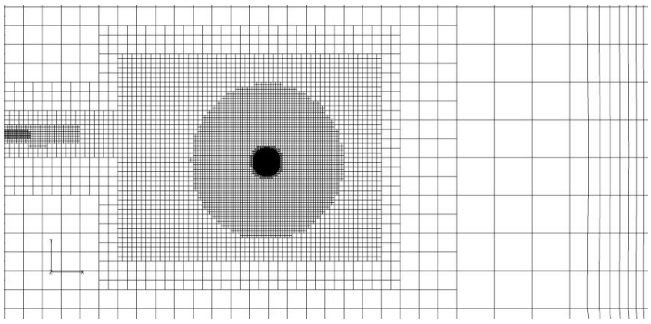

Figure 3: Inplane mesh distribution, P1S1

It should be noted that in both of the meshes, the foil surface resolution and prismatic layers' distribution (and also y^+=1) are the same, and the only difference between them is the resolution around the tip vortex trajectory.

Table 1: Cell size and mesh specifications

Name	Total number of Cells (M)	In-plane cell size (mm)	Streamwise cell size (mm)	Number of cells in vortex core
P1S1	8.3	0.125	0.25	8
P2S2Wake	44.3	0.062	0.125	16

5 SOLUTION PROCEDURE

In order to solve the governing equations, the OpenFOAM package, an open source code written in C++, is used to model and simulate fluid dynamics and continuum mechanics is employed [10].

For the current study, the velocity values on the faces of the computational cells are computed by second order upwinding schemes, linearUpwind. For other terms, e.g. turbulent kinematic energy and specific dissipation terms, second order linear scheme is employed. For unsteady simulations, a second order implicit scheme is used for time discretization. The time step is set fixed and small enough to ensure a maximum Courant number to be less than one everywhere in the computational domain for the period of collecting the results. All of the gradients have been corrected to include non-orthogonality effects. The pressure distribution in the vortex core region is presented by using the cavitation index,

$$\sigma = \frac{p\text{-}p_{sat}}{\frac{1}{2}\rho U_{ref}^2} \tag{23}$$

6 RESULTS

6.1 Vortex Properties

In Figures 4 and 5, tip vortex properties as predicted by different turbulence models for different spatial resolutions are presented. The comparison includes the variation of cavitation index, vortex trajectory, normalized axial velocity and turbulent kinematic viscosity. To determine the vortex core, a minimum pressure criterion is employed.

In both of the resolutions, and for all turbulence models tested here, negative pressure and also accelerated axial velocity is observed close to the foil, z/C <0.2. However, the difference between vortex roll-up and transportation is considerable which contributes to the vortex properties for z/C>0.2. In Figure 4, results of P1S1 simulations are presented. The results show over prediction of turbulent viscosity in RANS which damps the vortex after certain distance downstream of the foil. Figure 4(b) indicates that the tip vortex dissipates faster with standard SST compared to using other models. It is noted that after z/C>0.75, the vortex continuity breaks and oscillations on the vortex trajectory appears. For SST-RC, the oscillations start after z/C>1.1. This correlates to Figure 4(d) which represents the turbulent viscosity. As the highest turbulent viscosity is related to SST and then SST-RC, these models predict faster decay of vortex than SST-RC-Hellsten, and therefore sooner appearance of oscillations in vortex trajectory which relates to vortex breakdown. It is also clear from Figures 4(a) and 4(c) that the pressure and axial velocity in the vortex core quickly dissipates in all RANS models.

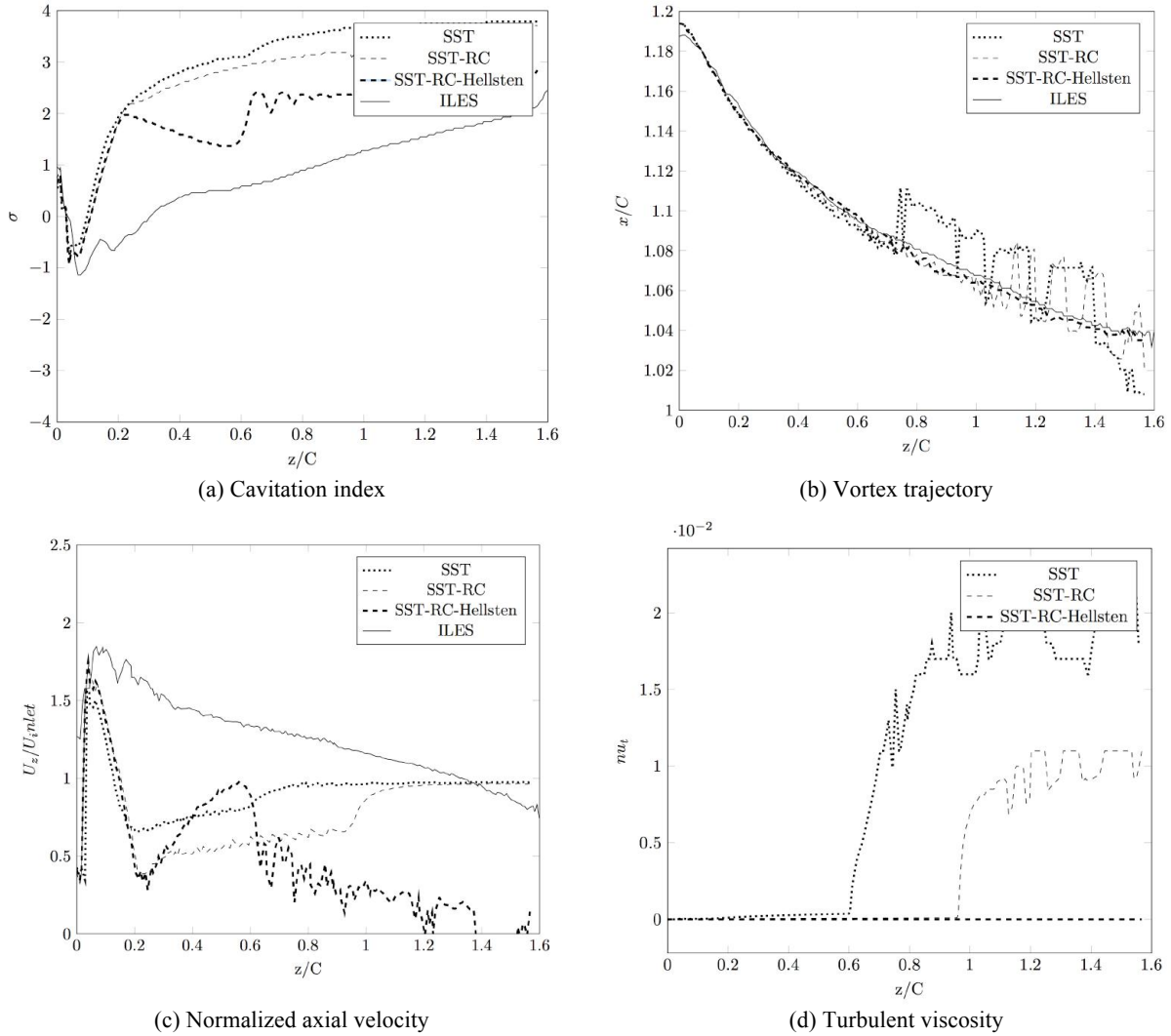

(a) Cavitation index

(b) Vortex trajectory

(c) Normalized axial velocity

(d) Turbulent viscosity

Figure 4: Variation of vortex core properties for different turbulence models, P1S1 resolution

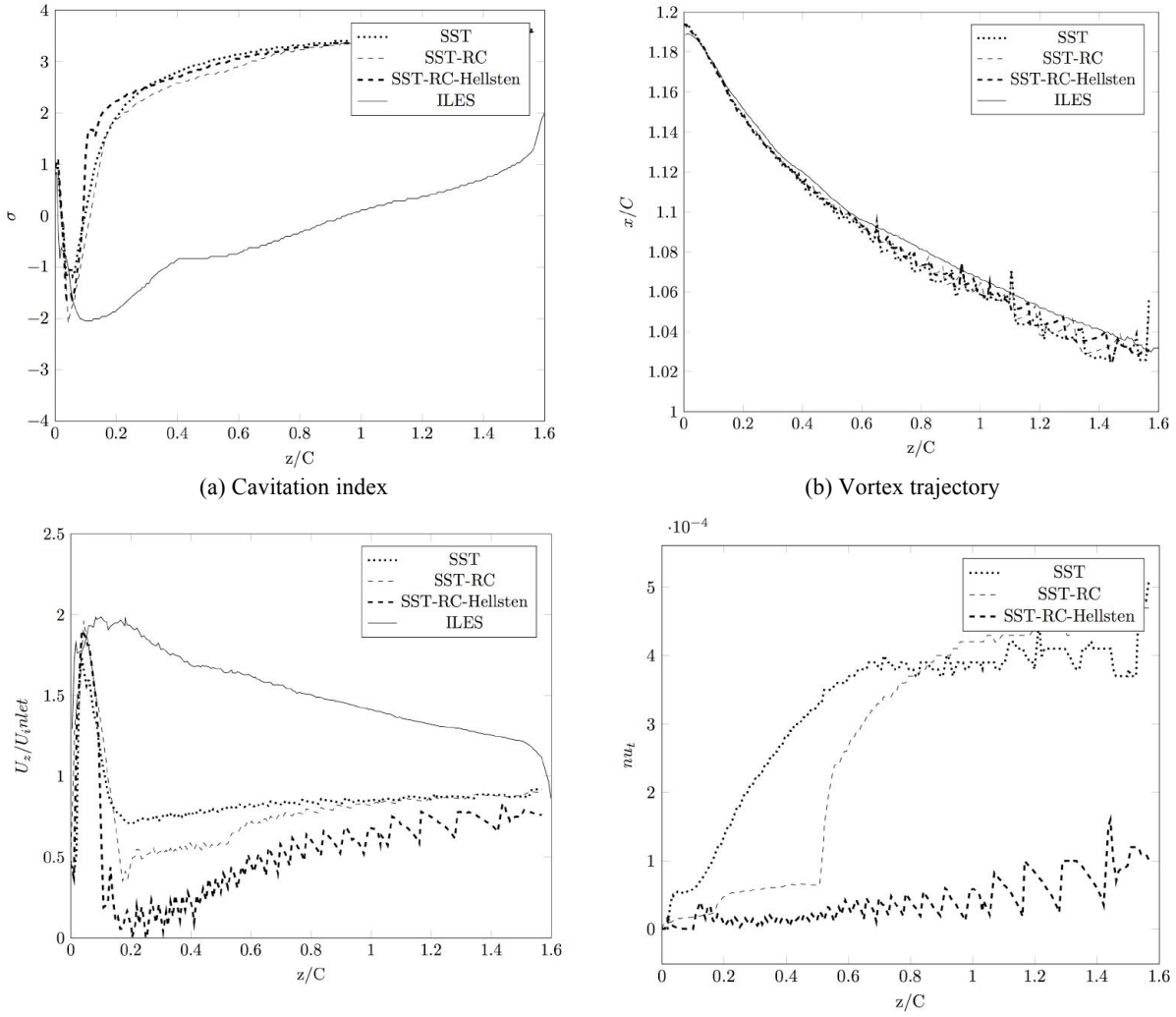

(a) Cavitation index

(b) Vortex trajectory

(c) Normalized axial velocity

(d) Turbulent viscosity

Figure 5: Variation of vortex core properties for different turbulence models, P2S2Wake resolution

When the resolution is increased, in ILES both the vortex strength and its size are increased. In RANS, the strength is also increased causing lower pressure at vortex core close to the tip but the size of the vortex is smaller, and vortex damps out faster, Figure 5(a). The vortex trajectory has less oscillations in the higher resolution, showing more continuous vortex pattern, Figure 5(b). Vortex core velocity predictions, Figure 5(c), show that all of the models predict the accelerated axial velocity, but in RANS as the vortex disappears, the core velocity also reduces. Similar trend in turbulent viscosity are observed for different curvature correction methods, Figure 5(d).

Thus, we conclude that none of the tested RANS models are able to predict the tip vortex correctly in the near field region, while ILES is better in predicting and transporting the vortex downstream in the region of interest, z/C<1.6.

6.2 Effects of Curvature Corrections

In Figure 6, the distributions of turbulent kinematic viscosity for different RANS models along with f_{r1} function of SST-RC model are presented at z/C=0.5 section. As it can be seen form the figure, the SST model is insensitive to the presence of the vortex, which leads to prediction of high turbulent viscosity at the vortex core region. The curvature correction models reduce the viscosity prediction at the vortex core. The comparison between RC and RC-Hellsten indicates that RC-Hellsten predicts lower viscosity at the vortex core region. It also indicates that RC-Hellsten leads to results which are sensitive to mesh variations.

The distribution of f_{r1} shows that in both resolutions the value of the function is very small, and close to zero in the vortex core region. It indicates that the curvature correction is acting correctly in lowering the production terms in the region where the vortex has evolved. Therefore, other parameters should be involved that lead to inaccurate prediction of the tip vortex. One of the parameters could be the contribution of boundary layer prediction.

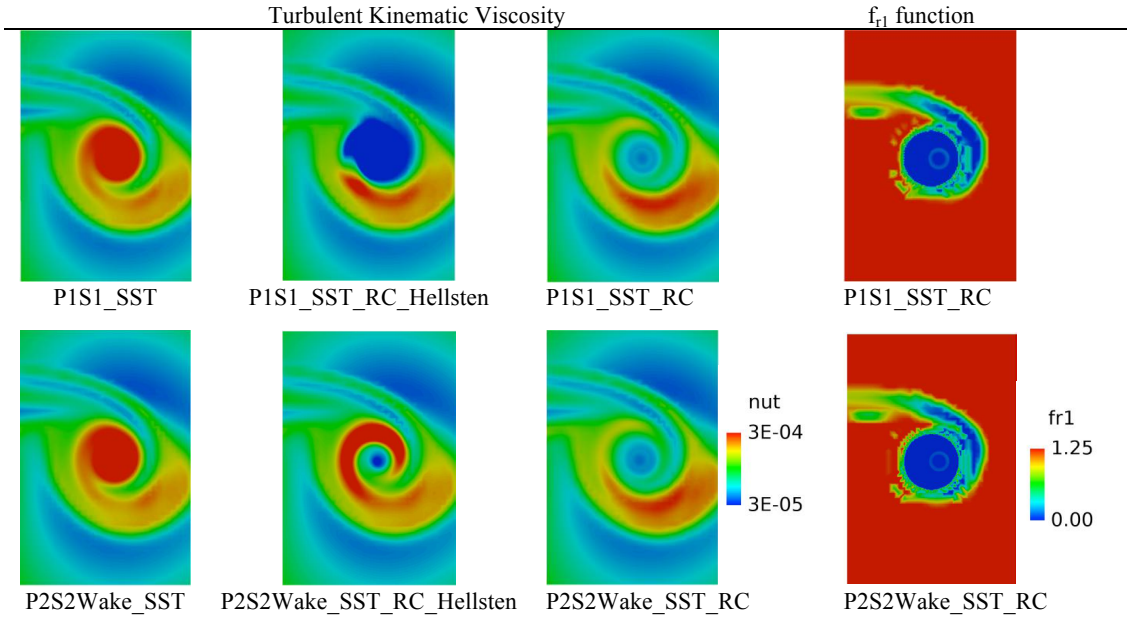

Figure 6: RANS turbulent viscosity, and RC function distributions at z/C=0.5

In Figure 7, velocity streamlines of SST-RC and ILES for P2S2Wake resolutions are presented. In frames (a) and (b) of the figure, the close up view of tip vortex are presented; the foil is colored with Cp distribution. The iso-surface of $p=p_{sat}$ is also presented with white shaded color to indicate the region with possible cavitation inception. In Figure 7(c), the isometric view of SST-RC is presented along with identifying the zoomed region. For this part, the streamlines are colored with turbulent viscosity.

Comparing ILES and SST-RC results, Figures 7(a) and (b), shows that in ILES the region with lower pressure is larger than SST-RC even though that SST-RC seems to have more concentrated negative Cp close to the tip; the vortex also starts closer to the tip and slightly further back in the SST-RC simualtion. At the bottom of the low pressure region in ILES, Figure 7(a), a high pressure region exists which forces the flow towards the tip vortex. This pressure field sucks more flow from upstream and pressure side to the surface of the foil

suction side and then towards the tip vortex which as a result leads to a stronger tip vortex prediction in ILES. One uncertainty here is the contribution of low-Reynolds RANS simulation on the boundary layer and therefore pressure field prediction. As it is mentioned in the mesh description section, the spatial resolution employed here have normal resolution $y^+<1$. The study to investigate other normal resolutions in RANS simulations are also conducted. The primary results show no improvement in RANS tip vortex prediction. However, further investigations is required in order to make a more precise conclusion.

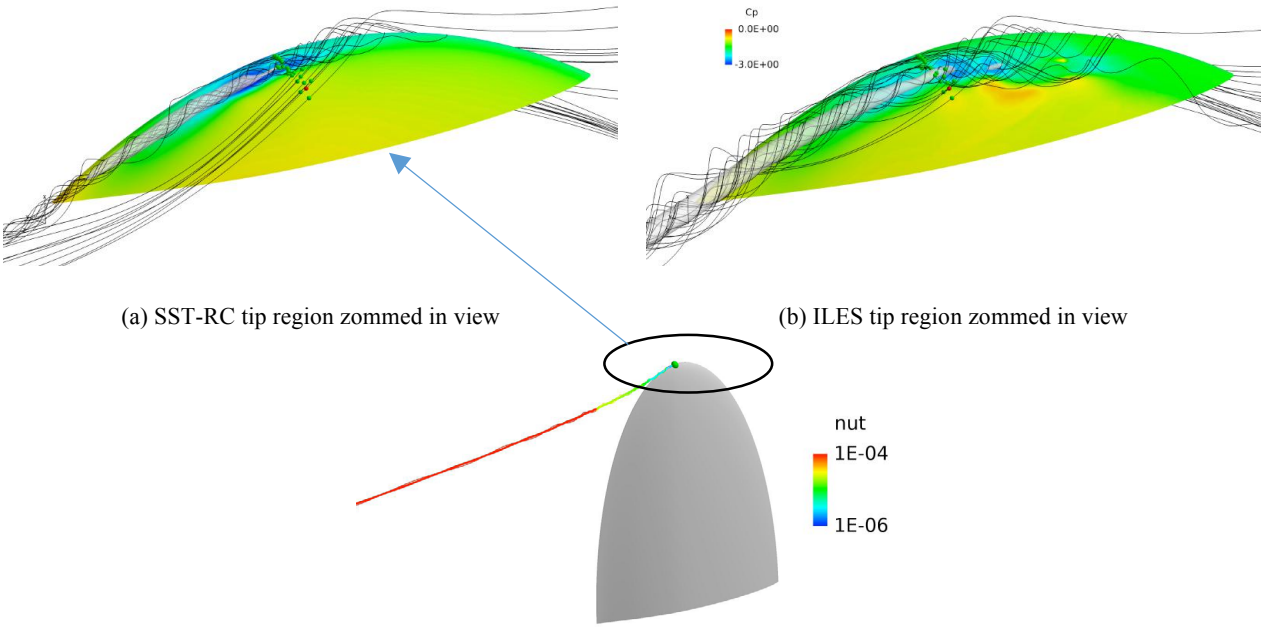

(a) SST-RC tip region zommed in view

(b) ILES tip region zommed in view

(c) SST-RC Isometric view

Figure 7: Flow streamlines for P2S2Wake resolution

6.3 Velocity Distributions

In Figures 8 and 9, the velocity distribution, at z/C=0.5 for P2S2Wake resolution are presented and compared with experiments. Comparison of normalized axial velocity comparison, Figure 8, show that only ILES could predict the accelerated axial velocity while the RANS methods employed here under predict the axial velocity at the vortex core. Under prediction is slightly higher for curvature correction methods.

SST | SST-RC-Hellsten | SST-RC | ILES | Exp

Figure 8: Comparison between RANS, ILES and experimental normalized axial velocity distributions, P2S2Wake resolution, z/C=0.5

In Figure 9, normalized in-plane velocity distributions are presented. Similar to the axial velocity comparison, ILES provides a more accurate prediction and matches better with the experimental PIV image. The RANS models fail in predicting the peak of the in-plane velocity which relates to the disablitity to transport the tip vortex until the z/C=0.5 section.

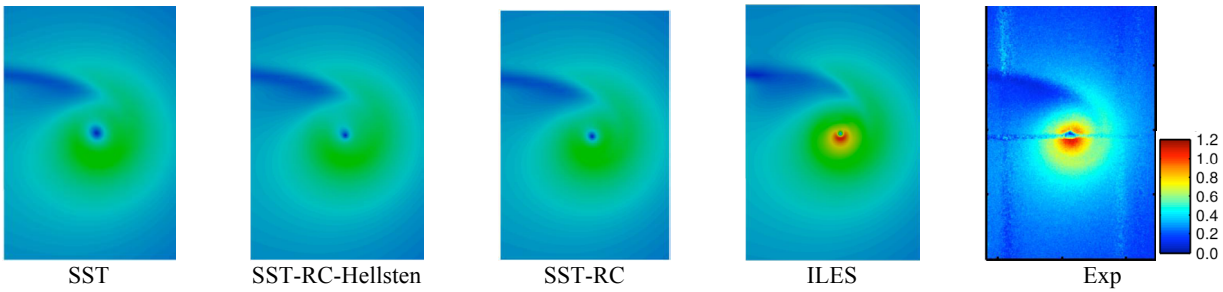

Figure 9: Comparison between RANS, ILES and experimental normalized inplane velocity distributions, P2S2Wake resolution at z/C=0.5

7 CONCLUSIONS

Tip vortex simulations of k-ω SST model and ILES are presented in this paper. For SST model, two curvature correction methods are also tested. To include the effects of the resolution on the tip vortex predictions, the simulations are carried ou on two different spatial resolutions.

ILES results show very good accuracy in prediction of vortex properties, e.g. axial and inplane velocity distributions. Tested RANS models fail in prediction of accelerated axial velocity. The vortex is much weaker in RANS, which is related to low flow suction into the vortex at the foil tip, and also the contribution of turbulent viscosity over-prediction. Figure 6 shows that the curvature correction methods reduce the turbulent viscosity at the vortex region. However, they could not improve the SST tip vortex predictions, as the results are also related to the flow properties, e.g. foil surface pressure distribution and boundary layer properties. Flow streamlines, Figure 7, show the contribution of suction side pressure field on the vortex formation. For SST-RC-Hellsten model the sensitivity of the turbulent viscosity prediction to the mesh resolution is higher than other RANS models tested. For future steps, it is suggested to test the effects of foil normal resolution, y^+, on the vortex formation and also interactions of the curvature correction methods with variation of y^+ for RANS.

8 ACKNOWLEDGEMENT

Financial support for this work has been provided by Rolls- Royce Marine through the University Technology Centre in Computational Hydrodynamics hosted at the Department of Shipping and Marine Technology at Chalmers University of Technology. The simulations were performed on resources at Chalmers Centre for Computational Science and Engineering (C3SE) provided by the Swedish National Infrastructure for Computing (SNIC).

REFERENCES

[1] Arndt, R., Arakeri, V. H. and H. Higuchi (1991). 'Some observations of tip-vortex cavitation'. Journal of Fluid Mechanics, 229, pp 269-289

[2] Asnaghi, A., Feymark, A., and Bensow, R. (2015). 'Numerical Analysis of Tip Vortex Flow'. Proceedings of the 19th Numerical Towing Tank Symposium (NuTTS'16), Oléron, French.
[3] Bensow, R. and Bark, G. (2010). 'Implicit LES prediction of the cavitating flow on a propeller'. J. Fluids Eng., 132(4).
[4] Zhang, B. L. , Lou, J., Kang, C. W., Wilson, A., Lundberg, J., Svennberg, U., and Bensow, R. (2014) 'CFD Modeling of Propeller Tip Vortex over Large Distances'; International Journal of Offshore and Polar Engineering (1053-5381). 24(3), p. 181-183
[5] Arndt, R., and Keller AP. (1992). 'Water Quality Effects on Cavitation Inception in a Trailing Vortex'. ASME. J. Fluids Eng.;114(3):430-438. doi:10.1115/1.2910049.
[6] Shen, Y., and Chahine, G. and Hsiao, C. and Jessup, S. (2001) 'Effects of Model Size and Free Stream Nuclei on Tip Vortex Cavitation Inception Scaling'. In: CAV 2001: Fourth International Symposium on Cavitation, June 20-23, 2001, California Institute of Technology, Pasadena, CA USA.
[7] Schot, J., (2014). 'Numerical study of vortex cavitation on the elliptical Ardnt foil'. MSc Thesis, TU Delft University.
[8] Bensow, R. and Liefvendahl, M. (2008). 'Implicit and explicit subgrid modeling in LES applied to a marine propeller'. AIAA-4144.
[9] Bensow, R. (2011). 'Simulation of the unsteady cavitation on the the Delft Twist11 foil using RANS, DES and LES'. Second International Symposium on Marine Propulsors. Hamburg, German.
[10] Abolfazl Asnaghi, 'Developing Computational Methods for Detailed Assessment of Cavitation on Marine Propellers', Licentiate Thesis, Department of Shipping and Marine Technology, Chalmers University of Technology
[11] Abolfazl Asnaghi, Andreas Feymark, Rickard Bensow, 'Shear Stress Effects in Cavitating Flows', 17th Numerical Towing Tank Symposium (NuTTS'14)
[12] Smirnov, P. E., and Menter, F. R., "Sensitization of the SST Turbulence Model to Rotation and Curvature by Applying the Spalart-Shur Correction Term," ASME Journal of Turbomachinery, Vol. 131, October 2009, 041010
[13] Hellsten, A., "Some Improvements in Menter's k-omega SST Turbulence Model," AIAA Paper 98-2554, June 1998.
[14] Mani, M., Ladd, J. A., and Bower, W. W., "Rotation and Curvature Correction Assessment for One- and Two-Equation Turbulence Models," Journal of Aircraft, Vol. 41, No. 2, 2004, pp. 268-273.
[15] Pennings, P. C. and Westerweel, J. and van Terwisga, T. J. C., (2015). 'Flow field measurement around vortex cavitation', Experiments in Fluids, Vol 56, No 11.
[16] Pennings, P. C., (2016). 'Dynamics of Vortex Cavitation'. Doctoral Thesis, TU Delft University.
[17] Arndt, R., and Keller AP. (1992). 'Water Quality Effects on Cavitation Inception in a Trailing Vortex'. ASME. J. Fluids Eng.;114(3):430-438. doi:10.1115/1.2910049.
[18] Arndt, R., and Maines, B. (1994). 'Viscous effects in tip vortex cavitation and nucleation', 20th Symp. on Naval Hydrodynamics. Santa Barbara, CA.